11th International Symposium on Turbulence and Shear Flow Phenomena (TSFP11)
Southampton, UK, July 30 to August 2, 2019

THE TRANSITION AND MIXING EFFICIENCY OF THE TURBULENT FARADAY INSTABILITY

Antoine Briard
CMLA, ENS Cachan, CNRS, Université Paris-Saclay,
94235 Cachan, France
antoine.briard@hotmail.fr

Benoît-Joseph Gréa
DIF, DAM, CEA, Arpajon, France
benoit-joseph.grea@cea.fr

Louis Gostiaux
LMFA UMR 5509 CNRS, Université de Lyon,
École Centrale 69130 Écully Lyon, France
louis.gostiaux@ec-lyon.fr

ABSTRACT

The interface between two miscible fluids in stable stratification can be destabilized by a vertical periodic forcing as a result of the Faraday instability. As a result, the turbulent mixing layer of size $L(t)$ grows as long as internal gravity waves are excited by the parametric resonances. Eventually, the instability saturates to a final size L_{sat} recently predicted and successfully assessed numerically for a wide range of parameters and initial conditions. The outcomes of this work are twofold: (i) We observe numerically the transition of the instability from a harmonic to a sub-harmonic regime, and characterise it as a transition to turbulence. (ii) We determine the mixing efficiency of the turbulent Faraday instability using the concepts of sorted density fields and background potential energy: notably, the cumulative mixing efficiency decreases with larger forcing intensity, irrespective of L_{sat}.

INTRODUCTION

The interface of a two layer system of immiscible fluids can be destabilized by a vertical periodic forcing and produce a great variety of structures as a result of the Faraday instability (Faraday, 1831). When miscible fluids are considered, a turbulent mixing zone of extent $L(t)$ can grow in size as long as internal gravity waves are excited by the parametric resonances (Zoueshtiagh *et al.*, 2009). Eventually, the instability saturates - since the mean density gradient decreases with time - to a size L_{sat} recently predicted in Gréa & Ebo Adou (2018) using notably a stability criterion and multiple-scale analysis: $L_{sat} = 2\mathscr{A}_t G_0(2F+4)/\omega^2$, where G_0 is the gravitational acceleration, F the forcing intensity, ω the forcing pulsation, and $\mathscr{A}_t$ the Atwood number. This prediction was successfully assessed numerically for a wide range of parameters and initial conditions.

In what follows, two features are addressed. First, the transition of the instability from a harmonic to a sub-harmonic regime was observed in Gréa & Ebo Adou (2018) in the homogeneous framework. In the full inhomogeneous system with the reservoirs of pure fluids, the *harmonic to sub-harmonic transition* is observed here as well starting from an interface. This transition is interpreted as a transition to turbulence with a noteworthy change in global anisotropy between the two regimes.

Secondly, we determine the mixing efficiency of the turbulent Faraday instability using the concepts of sorted density fields and background potential energy (Winters *et al.*, 1995). This allows us to understand why the final size of the mixing zone obtained numerically L_{end} always slightly exceeds the prediction L_{sat}.

High resolution direct numerical simulations (DNS) of the Navier-Stokes Boussinesq equations are performed with 1024^3 points using a pseudo-spectral code in a triply-periodic box of size 2π. The kinetic energy is initially zero and is fully created by the instability; the kinematic viscosity is set to $\nu = 10^{-4}$ and the concentration variance is injected at small scales to disturb the initial interface. Further details can be found in Briard *et al.* (2019), and parameters are gathered in Table 1.

Table 1: Parameters of the 1024^3 DNS with $\nu = \kappa = 10^{-4}$, ordered by increasing F. Forcing intensity F; Atwood number $\mathscr{A}_t$; Pulsation ω; Gravitational acceleration G_0; Final cumulative mixing efficiency η_b^c.

Name	F	$\mathscr{A}_t$	ω	G_0	η_b^c
F055A015	0.55	0.015	3.46	65.15	0.420
F07A045	0.7	0.045	4.29	65.15	0.410
F1A01	1.0	0.01	0.7	10.0	0.415
F1A02	1.0	0.02	1.0	10.0	0.420
F1A1	1.0	0.1	2.2	10.0	0.413
F2A01	2.0	0.01	0.8	10.0	0.391
F5A01	5.5	0.01	1.0	10.0	0.254
F8A02	8.0	0.02	2.0	10.0	0.198

THE TRANSITION

Within the rapid acceleration model (Gréa, 2013) where viscous effects and non-linearities are discarded in order to keep only production terms and the interaction between turbulence and mean fields, the fluctuating concentration $c = C - \overline{C}$ verifies a classical Mathieu equation (Gréa & Ebo Adou, 2018)

$$\frac{\partial^2 \hat{c}}{\partial t^2} + N^2 \sin^2(\theta)(1 + F\cos(\omega t))\hat{c} = 0, \qquad (1)$$

whose stability diagram is given in figure 1. Here, θ is the angle between the vertical axis and the wavevector $\boldsymbol{k}$, $N = \sqrt{2\mathscr{A}_t G_0 / L}$ is the stratification frequency, $\hat{c}$ is the Fourier transform of c, and $\overline{C}$ is the horizontally-averaged concentration field. For a given initial condition at a fixed F, a whole horizontal segment delimited by two crosses is excited: the l.h.s. extremity corresponds to $\theta = 0$, and the r.h.s. to $\theta = \pi/2$. Hence, at each time, the extent of the segment is $[0; (N/\omega)^2]$, where, the r.h.s. extremity $(N/\omega)^2$ corresponds to the mixing zone size $L(t)$. Two cases should be distinguished: the instability is not triggered (red cross), meaning that the initial excited segment is entirely in the grey stable region at left. The second case is when $(N/\omega)^2$ falls beyond the marginal stability curve, meaning that some θ-modes are excited (green, yellow and blue crosses). Hence $L(t)$ will grow in size and thus $(N/\omega)^2$ will decrease toward the left of the diagram, indicated by arrows. If $(N/\omega)^2$ is initially in the harmonic tongue, then the harmonic to sub-harmonic transition can be observed. More precisely, we define the time at which the transition occurs when all harmonic modes have become stable, corresponding to the mixing layer size $L = L_{tr}$.

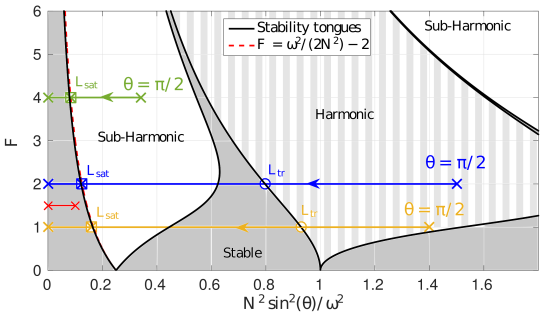

Figure 1: Mathieu diagram: stability curves (black) separate stable regions (grey) from harmonic and sub-harmonic unstable regions. The marginal stability curve is displayed as a dashed red curve. Various initial conditions, delimited by crosses $\times$ (from $\theta = 0$ to $\theta = \pi/2$), are discussed in the text.

We are now interested in the time evolution of the mixing zone size $L(t)$: four runs are presented in figure 2 for $F = 1$ and $F = 2$. These configurations have almost the same prediction L_{sat}, see Table 1, and hence comparable final size L_{end} in the asymptotic state, but different transients. The transition size L_{tr} corresponds to the size from which harmonic modes are no longer excited, as shown in figure 1. The values of L_{tr} are quite similar for the runs presented in figure 2: $L_{tr} \simeq 0.44$, reported as $-\cdot$ horizontal lines. Since all modes $\theta \in [0; \pi/2]$ are excited at each time, this value of L_{tr} can be crossed several times, like for $F = 1$, or only once, like for $F = 2$. The last time for which L_{tr} is crossed corresponds to the *harmonic to sub-harmonic transition*, and is indicated by a vertical dashed line: for instance, this is at $\omega t = 44$ for run F1A01. The transition occurs much more rapidly for $F = 2$ than $F = 1$: this is expected since with a larger forcing intensity F, $L(t)$ grows more rapidly. On the contrary, at $F = 1$, the transition is delayed with an increasing Atwood number.

Note that for all runs, the final size of the mixing zone L_{end} exceeds the prediction by roughly 20%, and this feature, already observed in Gréa & Ebo Adou (2018), will be explained in the next section.

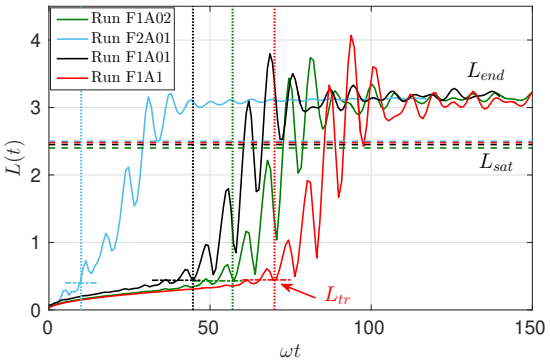

Figure 2: Mixing zone size $L(t)$; horizontal dashed lines correspond to the prediction L_{sat}. Vertical dashed lines indicate the separation between the harmonic and sub-harmonic regimes.

From figure 2, the transition is hardly visible on $L(t)$, which should oscillate in the harmonic regime twice as fast as in the sub-harmonic one. The Fourier transform of $\dot{L}$ reveals an intense peak at $f = \omega/(2\pi)$ corresponding to the sub-harmonic regime, and a second moderate peak at $f = \omega/\pi$ corresponding to the harmonic regime. A more convincing proof is nevertheless proposed by analysing the global anisotropy of the concentration field. We use the dimensionality parameter $\sin^2\gamma$, which reflects the directional anisotropy of a scalar field for statistically axisymmetric configurations (Gréa, 2013):

$$\sin^2\gamma = \frac{\int_0^\infty \int_0^\pi \mathscr{E}_{cc}(\boldsymbol{k},t)\sin^3\theta \,\mathrm{d}\theta\,\mathrm{d}k}{\int_0^\infty \int_0^\pi \mathscr{E}_{cc}(\boldsymbol{k},t)\sin\theta \,\mathrm{d}\theta\,\mathrm{d}k}. \qquad (2)$$

Here, $\mathscr{E}_{cc}(\boldsymbol{k}) = \mathscr{E}_{cc}(k,\theta)$ is the spectral two-point concentration correlation: note that for an isotropic state, $\sin^2\gamma = 2/3$. The time evolution of $\sin^2\gamma$ is presented in figure 3 for runs F1A01 and F2A01. For $F = 1$, the transition is clearly visible, with the period in the sub-harmonic regime being twice as large as in the harmonic one. Anisotropy is maximal in the harmonic regime and increases ($\sin^2\gamma$ departs from $2/3$): since the limit $\sin^2\gamma = 0$ corresponds to sheet-like structures, the information provided by $\sin^2\gamma$ is consistent with structures being more and more tilted toward the horizontal while approaching the transition. Then,

global anisotropy decays ($\sin^2\gamma$ tends to $2/3$) after the transition and during the sub-harmonic regime due to more intense turbulent transfers. The increase of $\sin^2\gamma$ is consistent with structures being dominantly vertically aligned and stretched. In the asymptotic state, $\sin^2\gamma$ roughly oscillates close the isotropic value $2/3$. The scenario is a bit different for $F=2$: since the harmonic regime is very short as noted above, the concentration field is less anisotropic because structures do not have time to be significantly tilted. In the asymptotic state, the concentration field is slightly more anisotropic with $F=2$ than for $F=1$ because the instability was much sorter, and thus less mixing occurred.

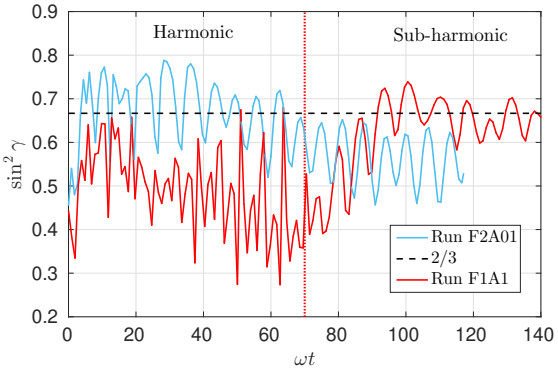

Figure 3: Concentration global anisotropy indicator $\sin^2\gamma$; the vertical dashed line indicates the separation between the harmonic and sub-harmonic regimes.

We pursue our analysis of one-point statistics to better characterise the transition between the harmonic and sub-harmonic regimes. Previously, it appeared that the growth of the mixing zone mainly occurs in the sub-harmonic regime, whereas global indicators revealed that the harmonic regime was more anisotropic than the sub-harmonic one. Hence, there is a severe change in the dynamics at the transition. Hence, the Froude number $Fr=\varepsilon_{uu}/(NK_{uu})$ - where $K_{uu}=\langle u_iu_i\rangle/2$ is the kinetic energy and ε_{uu} its dissipation rate - and the integral Reynolds number $Re_L=K_{uu}^2/(\nu\varepsilon_{uu})$ are investigated in figure 4.

The time evolution of Fr is presented in figure 4 for runs F1A01 et F2A01. In the harmonic regime for $F=1$, Fr is rather small because of the strong stratification. Then, from the transition and during the sub-harmonic regime, Fr significantly increases because turbulent exchanges become more intense, consistently with the strong growth of the mixing zone size $L(t)$ observed previously. In the asymptotic state, Fr decreases with the decay of the turbulence intensity due to the saturation of the instability. For $F=2$, the harmonic regime is almost not visible as pointed out previously. The Froude number strongly increases towards larger values than for $F=1$, as expected since production is more intense. The instability saturates more rapidly as well, thus shortening the turbulent sub-harmonic regime.

The Reynolds number, displayed in figure 4 as well, also shows the great enhancement of turbulence after the transition. From almost 0, it reaches its maximum value $\simeq 9.10^3$ in the sub-harmonic regime, and then settles around 10^3 in the asymptotic saturated state. The intensification of turbulent features and the creation of small scales participate as well to the reduction of global anisotropy from the transition, as observed in figure 3 for $F=1$.

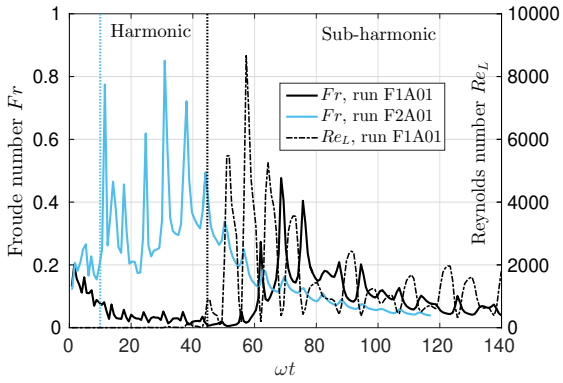

Figure 4: Turbulent quantities for runs F1A01 (black) and F2A01 (light blue): Fr on the left y-axis, and Re_L on the right one for run F1A01.

MIXING EFFICIENCY

Now that the transition between the harmonic and sub-harmonic regimes has been characterised and interpreted as a transition to a turbulent state where the mixing zone grows significantly, we aim at quantifying the irreversible mixing of the flow using mixing efficiency and background potential energy (Winters *et al.*, 1995; Peltier & Caufield, 2003).

The total potential energy being $E_p=\int\rho' gz\mathrm{d}V$, and having $\rho'\sim 2\mathscr{A}_t\rho_0 c$ within the Boussinesq approximation, we refer hereafter unambiguously to the normalized potential energy per unit surface as

$$e_p(t)=\frac{E_p(t)}{4\pi^2\rho_0}=2\mathscr{A}_tG_0\int\overline{C}(z,t)z\mathrm{d}z. \tag{3}$$

Since e_p can be modified by adiabatic processes (reversible mixing), we are interested in the sorted concentration field $C(z^*)$ which depends only on the probability density function (PDF) of the concentration field $f(C)$. z^* is the position in the state of minimum potential energy attainable through an adiabatic redistribution of C. This minimum potential energy is the *background potential energy* defined as

$$e_p^b(t)=2\mathscr{A}_tG_0\int_{z_{min}}^{z_{max}}C(z^*)z^*\mathrm{d}z^*, \tag{4}$$

and reflects the amount of gravitational potential energy e_p expanded in mixing the two fluids. The reference state is computed from the PDF as in Davies Wykes & Dalziel (2014) according to $z^*(C)=z_{min}+(z_{max}-z_{min})\int_0^C f(x)dx$ where z_{min} and z_{max} are the boundaries of the fluid domain. Here, the PDF is built with 4096 points. Then, the *available potential energy* $e_p^a=e_p-e_p^b$ corresponds to the energy that would be released during an adiabatic transformation toward the background state. In other words, e_p^a is the

fraction of total potential energy which can be converted into e_p^b through irreversible mixing.

We are now interested in the energy contents of run F1A01. The PDF of the concentration field is presented in the inset of figure 5 at three different times. Initially, $f(C)$ is sharply peaked around $C = 0$ and $C = 1$. At $\omega t = 69$ when $L(t)$ is maximum, there is a noteworthy bump around $C = 0.5$ reflecting that there is more and more mixing. The time evolution of the three potential energies is displayed in figure 5 for the same run. The background potential energy (red) increases monotonically as the irreversible mixing of the two fluids progresses. Notably, e_p^b increases substantially only after the transition, and this is verified for all runs. The gain of background potential energy over the whole simulation can be evaluated as $\Delta e_p^b = \mathscr{A}_t G_0(\tilde{L}_{end}^2 - L_0^2)/12$, where $\tilde{L}_{end}$ is the final mixing zone size computed with the sorted profile $C(z^*)$. For run F1A01, $\Delta e_p^b = 0.079$, which is in good agreement with the plot of figure 5. The gain in background potential energy varies by more than one order of magnitude depending on the control parameters.

An additional outcome is that available potential energy (blue) is maximal in figure 5 when $L(t)$ reaches the saturation prediction L_{sat} at $\omega t \simeq 70$. This explains why in Gréa & Ebo Adou (2018) and in figure 2 the final size L_{end} always exceeds the prediction. Indeed, L_{sat} corresponds only to the *saturation* of the instability. After the saturation, the e_p^a is partially released in the flow as e_p^b. This additional background potential energy eventually makes L slightly larger than L_{sat} despite the saturation of the instability.

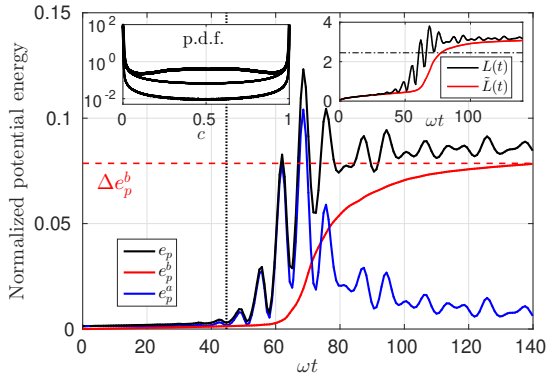

Figure 5: Total, background and available potential energies e_p, e_p^b, and e_p^a for run F1A01. First inset: PDF at time $t = 0$, $\omega t = 40$, and $\omega t \simeq 69$ when $L(t)$ is maximal. Second inset: unsorted $L(t)$, sorted $\tilde{L}(t)$.

We now move on with estimating the *mixing efficiency* of our turbulent instability, if any sense can be given to an instantaneous mixing efficiency in a framework with a periodic forcing. We consider three different possibilities to compute the mixing efficiency hereafter. A first definition is borrowed from Venayagamoorthy & Koseff (2016), where the mixing efficiency reads $\eta_{PE} = \varepsilon_{PE}/(\varepsilon_{PE} + \varepsilon_{uu})$, where $\varepsilon_{PE} = N^2 \varepsilon_{cc} (d\overline{C}/dz)^{-2}$, and is like a flux Richardson number. This definition is more robust than others which rely on the scalar flux $\langle u_3 c \rangle$ that accounts for reversible mixing. Nevertheless, this definition intrinsically takes into account both reversible and irreversible mixing since it is not based on $C(z^*)$. The instantaneous mixing efficiency η_{PE} is given in figure 6 for run F1A01. Oscillations are quite wide because ε_{uu} and ε_{PE} oscillate in phase opposition. After the transition, η_{PE} decays due to the strengthening of the turbulence. In the saturated state, η_{PE} roughly settles around 0.35. The second definition can be found in Peltier & Caufield (2003); Davies Wykes *et al.* (2015) and is based on the background potential energy. The instantaneous mixing efficiency reads $\eta_b = \varepsilon_b/(\varepsilon_b + \varepsilon_{uu})$, where ε_b is the dissipation rate of the background potential energy density. The time evolution of η_b in figure 6 is quite similar to the one of η_{PE}, but with oscillations of smaller amplitudes. This is expected since reversible mixing is excluded while using ε_b rather than ε_{PE}.

It becomes clear with figure 6 that there is no real meaning to an instantaneous mixing efficiency in a periodically forced system. Instead, we compute the cumulative mixing efficiency (Peltier & Caufield, 2003)

$$\eta_b^c(t) = \frac{\int_0^t \varepsilon_b(t')\mathrm{d}t'}{\int_0^t \varepsilon_b(t')\mathrm{d}t' + \int_0^t \varepsilon_{uu}(t')\mathrm{d}t'}. \tag{5}$$

This definition provides a smooth time evolution compared to the previous definitions η_{PE} and η_b. The final value for run F1A01 is $\eta_b^c = 0.415$, which is close to the final value of η_b: final values of η_b^c for the other runs are gathered in Table 1 as well. It is worth noting that η_b^c is much less sensitive to the control parameters than Δe_p^b. An interesting finding is that the cumulative mixing efficiency tends to decrease with larger F, irrespective of L_{sat}. Indeed, with larger F, the instability saturates rapidly and thus there is less time for irreversible mixing.

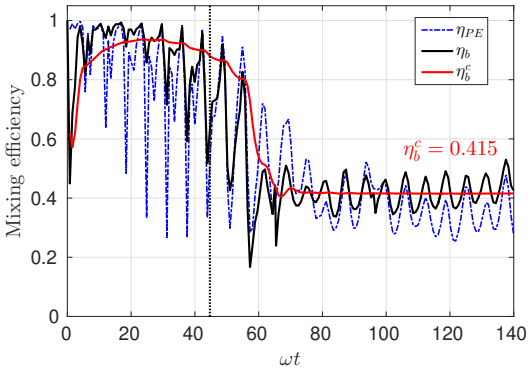

Figure 6: Instantaneous mixing efficiencies η_{PE} (blue) and η_b (black), along with the cumulative mixing efficiency η_b^c (red) for run F1A01.

The particularities here are that the flow is unsteady because of the periodic forcing, and that most of the mixing happens in the sub-harmonic regime, which represents a short time of the simulation, and in a small domain between the two reservoirs of pure fluids. Although there is a conceptual complexity of evaluating mixing efficiency in a transitory and periodically forced system, the different estimations tend to qualify the Faraday instability as an efficient mixing process.

CONCLUSION

When a two layer system of stably stratified miscible fluids is accelerated vertically and periodically, a turbulent mixing zone may develop as a result of the Faraday instability. It eventually reaches a final state at the end of parametric resonances, where the final saturated size L_{sat} was predicted in Gréa & Ebo Adou (2018) and assessed for a wide range of parameters.

Here, we have observed numerically for the first time the transition of the miscible Faraday instability from a harmonic to a sub-harmonic regime in the full inhomogeneous system starting from an interface. Our primary goal was to characterize this transition. Therefore, we identified a robust scenario describing the dynamics of structures. In the harmonic regime, the fields are highly anisotropic because vertically elongated structures develop. A sudden decrease in anisotropy occurs at the transition since turbulence is strongly enhanced, which creates small scales that partially restore isotropy. Then, in the sub-harmonic regime, global anisotropy slightly increases because structures align again in the vertical direction.

One-point turbulent quantities such as the Froude and Reynolds numbers confirm that the harmonic to sub-harmonic transition is a sharp transition to turbulence. Regarding the mixing zone size $L(t)$, it strongly increases only from the transition. It has been shown that for similar final states L_{end}, various transients can be observed depending on the control parameters, with or without harmonic regimes.

Afterwards, we determined the time evolution of the background potential energy e_p^b which is a measure of the irreversible mixing of the flow, starts only after the transition. A major outcome of this analysis is that at saturation of the instability, available potential energy e_p^a is partially released as background potential energy e_p^b in the flow: this additional irreversible mixing causes L to grow beyond L_{sat}. This notably explains why in Gréa & Ebo Adou (2018) the final size obtained numerically L_{end} always exceeds the prediction L_{sat}.

Finally, three different definitions of the mixing efficiency were compared: we argue that it might not be relevant to investigate instantaneous mixing efficiencies since our flow is highly unsteady and mixing occurs within a limited time and space domain. The cumulative mixing efficiency η_b^c however has a smooth evolution. It is worth noting that its final value decreases with larger forcing parameters F, irrespective of L_{sat}: indeed, with larger F, the instability saturates quickly and the mixing process is shortened.

REFERENCES

Briard, A., Gréa, B.-J. & Gostiaux, L. 2019 Harmonic to subharmonic transition of the faraday instability in miscible fluids. *Physical Review Fluids* **4**, 044502.

Davies Wykes, M. S. & Dalziel, S. B. 2014 Efficient mixing in stratified flows: experimental study of a rayleightaylor unstable interface within an otherwise stable stratification. *Journal of Fluid Mechanics* **756**, 1027–1057.

Davies Wykes, M. S., Hughes, G. O. & Dalziel, S. B. 2015 On the meaning of mixing efficiency for buoyancy-driven mixing in stratified turbulent flows. *Journal of Fluid Mechanics* **781**, 261–275.

Faraday, M. 1831 Xvii. on a peculiar class of acoustical figures; and on certain forms assumed by groups of particles upon vibrating elastic surfaces. *Philosophical Transactions of the Royal Society of London* **121**, 299–340.

Gréa, B.-J. 2013 The rapid acceleration model and the growth rate of a turbulent mixing zone induced by rayleigh-taylor instability. *Physics of Fluids* **25**, 015118.

Gréa, B.-J. & Ebo Adou, A. 2018 What is the final size of turbulent mixing zones driven by the faraday instability. *Journal of Fluid Mechanics* **837**, 293–319.

Peltier, W. R. & Caufield, C. P. 2003 Mixing efficiency in stratified shear flows. *Annual Review of Fluid Mechanics* **35**, 135–167.

Venayagamoorthy, S. K. & Koseff, J. R. 2016 On the flux richardson number in stably stratified turbulence. *Journal of Fluid Mechanics* **798**, R1.

Winters, K., Lombard, P. N., Riley, J. J. & D'Asaro, A. 1995 Available potential energy and mixing in density-stratified fluids. *Journal of Fluid Mechanics* **289**, 115–128.

Zoueshtiagh, F., Amiroudine, S. & Narazanan, R. 2009 Experimental and numerical study of miscible faraday instability. *Journal of Fluid Mechanics* **628**, 43–55.